Mechanical, fracture and thermal characterization of post-cured hybrid epoxy nanocomposites reinforced with Graphene nanoplatelets and h-Boron Nitride

Mantesh C. Choukimath, N. R. Banapurmath*
School of Mechanical Engineering, KLE Technological University, Hubballi, Karnataka, India.
mantesh@kletech.ac.in, https://orcid.org/0000-0001-7696-6037
nrbanapurmath@kletech.ac.in, https://orcid.org/0000-0002-1280-6234

M. A. Umarfarooq
Center of Excellence in Material Science, School of Mechanical Engineering, KLE Technological University, Hubballi, Karnataka, India.
umarfarooq.ma@gmail.com, https://orcid.org/0000-0002-9369-7913

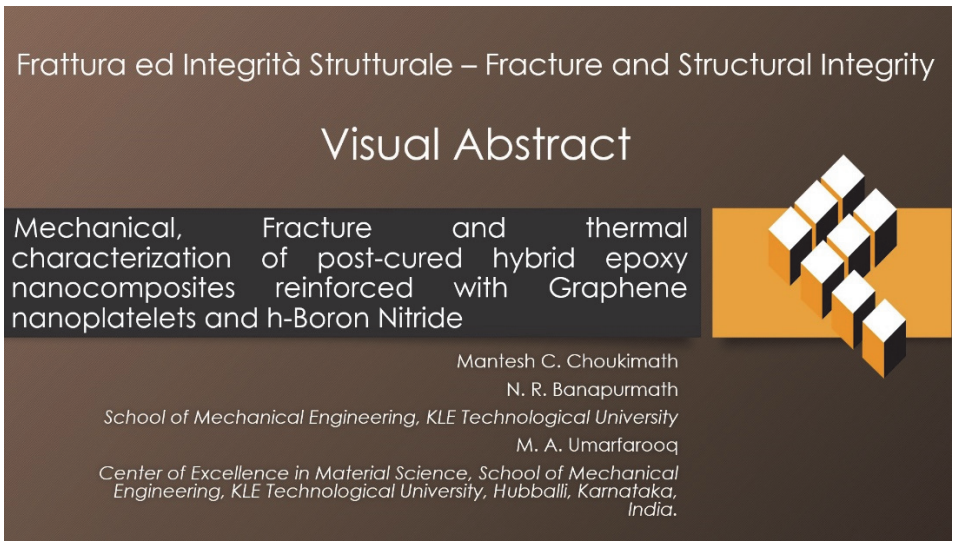

Citation: Choukimath, M. C., Banapurmath, N. R., Umarfarooq, M. A., Mechanical, Fracture and Thermal Characterization of Post-Cured Hybrid Epoxy Nanocomposites Reinforced with Graphene Nanoplatelets and h-Boron Nitride, Fracture and Structural Integrity, 71 (2025) 22-36.

Received: 12.08.2024
Accepted: 06.10.2024
Published: 08.10.2024
Issue: 01.2025

KEYWORDS. Nanocomposites, Post-curing, Epoxy, GNP, h-BN, Mechanical and thermal properties.

INTRODUCTION

Epoxy resins were first synthesized in the 1930s, and early applications in coatings, adhesives, and electrical insulation were found. In the 1950s, their use expanded into composite materials, particularly for aerospace and military applications. Since then, the versatility and durability of epoxy have led to its widespread use in various polymer applications, including construction, automotive, and electronics [1, 2].

Epoxy resins have a variety of inherent qualities due to the highly reactive epoxy groups in their terminal chains. These outstanding qualities make them excellent for use in high-performance applications. Epoxy systems based on diglycidyl ether of bisphenol A (DGEBA) are widely utilized in the plastics sector due to their superior structural qualities, such as high chemical resistance, low shrinkage, and better coating capabilities. [3, 4]. The intrinsic brittleness of thermosetting polymer materials is typically attributed to the high density of cross-linking that occurs during the curing process. Thus, the properties of the cured composite are highly influenced by the type and chemical structure of the monomer and the curing agent used during the curing process. Also, the curing conditions, such as curing time, temperature, and pressure, play a vital role in the synthesized composite [5, 6].

Optimizing the curing process can enhance the final properties of an epoxy system. Lower curing temperatures can result in a thermosetting resin with a lower Tg, as some reactive groups from the epoxy resins or hardeners may not completely react. Post-curing is generally performed at a temperature higher than the initial curing temperature to achieve optimal cross-linking. This process leads to a resin with superior mechanical properties and low shrinkage, which improves stability. Additionally, the resultant resins can offer better resistance in surface coatings and better adhesion strength making them ideal for various industrial applications, including paints, adhesives, and high-performance membranes [7, 8]. It is also known that polymeric-based nanocomposite materials cannot be used for high-performance applications because of their limited properties. This limitation can be overcome by introducing organic/inorganic nanoparticles. GNPs offer significant potential for multifunctional properties. These GNPs are made up of graphene sheet stacks of platelet structure, similar to the planar form found in carbon nanotubes. GNPs can improve the mechanical properties of matrix materials, including stiffness, strength, and surface hardness [9]. h-BNs have tremendous potential for multifunctional applications. h-BN is constructed of minute hexagonal layers that are physically similar to graphene but contain alternating boron and nitrogen atoms. This unusual structure gives h-BN outstanding thermal and electrical insulating qualities. Furthermore, h-BN nanofillers can improve the mechanical properties of the matrix material by enhancing heat conductivity, lubricity, and resistance to wear and corrosion [10]. The ultrasonication process can be used to achieve an optimal distribution of nanoparticles (NPs) within the base material, ensuring the maximum dispersion of NPs in the holding matrix [11]. FEM analysis with Ansys software is critical for designing polymer nanocomposites because it allows simulation of their mechanical and thermal properties at the microstructural level. Ansys optimizes material composition, predicts performance, and identifies probable failure areas by simulating the interactions between the polymer matrix and nanofillers [15, 23, 24].

Olszowska et al. found that composites containing GNPs and micro-sized carbon foam in an epoxy matrix improved thermal conductivity by 20%, mechanical strength by 15%, and friction coefficient by 30% [9]. Choukimath et al. reported an increase of 49.25% in the tensile strength of h-BN based epoxy nanocomposites prepared with varying compositions of h-BN from 0.1 to 0.5 wt% [12]. Jahani et al. examined the effect of post-curing on the mechanical properties of a structural epoxy glue at various temperatures. Their work concluded that curing and post-curing below the adhesive's Tg improve mechanical characteristics, whereas temperatures over Tg cause degradation. Testing temperatures above 20°C have a negative impact on tensile and compressive characteristics, with considerable reductions reported at temperatures near and beyond Tg [13]. Min, C. et al. describe the creation of a three-dimensional interconnected graphene architecture (3DGA) reinforced epoxy composite. Using resin transfer molding and an in-situ ultrasonic technique, the 3DGA was evenly distributed within the epoxy matrix, resulting in improved thermal stability, mechanical strength, and tribological properties. Compared to typical graphene oxide composites, the 3DGA/EP composite showed a 27.1°C rise in glass transition temperature, a 41.1% increase in tensile strength, and a 38.1% decrease in wear rate, indicating its potential for high-performance applications [14]. Choukimath et al. reported a significant increase in tensile, flexural load bearing, and thermal stability of GNP and h-BN embedded epoxy nanocomposites. The inclusion of GNPs increased the load-bearing capacity by 265% and the flexural strength by 165% at a concentration of 0.2 wt%. When coupled with h-BN at 0.6 wt%, the nanocomposite exhibited increased thermal stability, withstanding higher temperatures as confirmed by thermogravimetric analysis. These enhancements make the nanocomposite suitable for high-temperature applications, including compressor blades in gas turbine engines[15].

In this study, a comprehensive investigation is conducted on hybrid epoxy nanocomposites reinforced with GNP) and h-BN nanofillers, which are subjected to various post-curing temperatures. Unlike prior studies, the synergistic effects of dual nanofiller reinforcement and different post-curing temperatures on the mechanical, thermal, and fracture properties of the composites are examined. Additionally, experimental data combined with ANSYS simulation provides strong confirmation of the observed behaviors, revealing new understandings for enhancing material properties in high-performance applications. Subsequent sections provide information on materials, methodology, specimen preparation, experimental details, test procedure and analysis.

MATERIAL AND METHODOLOGY

The epoxy matrix material (branded as Lapox-L12 and paired with K6 hardener) used in this study was sourced from Atul Private Limited's Polymer division Gujarat, India. The GNPs and h-BNs used in the study had a minimum purity of 99.5% and 99.9% respectively. The properties of GNP and h-BN used are displayed in Tab. 1.

Properties	GNP	h-BN
Density (g/cm3)	2.3	2.9
Ultimate Tensile Strength (MPa)	5000	83
Young's Modulus (GPA)	1000	37
Poisson's Ratio	0.19	0.24
Melting Point (°C)	>3600°C	2527°C
Dimensions (nm)	3	60

Table 1: Properties of GNP and h-BN nanofillers.

PREPARATION OF SPECIMENS

The nano-composites were synthesized using an in-situ polymerization process. Three types of epoxy-based nanocomposites were prepared, one with GNPs, another with h-BNs and the third with a combination of both GNPs and h-BNs. The nanocomposite composition is displayed in Tab. 2. After adding the appropriate amount of nanofillers and epoxy matrix by weight percentage, the mixture was subjected to sonication for 60 minutes to improve the nanofillers dispersion in the matrix [15]. Further, 10% by weight of aliphatic polyamine hardener (K6) was added to the epoxy base to initiate the polymerization process. This final mixture was cast into the aluminum mold of size 230 mm × 164 mm × 3 mm. These cast plates were allowed to cure for 24 hours. After the curing process, the composite plates were removed from the molds and were cut to the ASTM specifications for different test procedures. Further, these prepared composites were subjected to post-curing in a hot air oven for 120 minutes at different post-curing temperatures (80°C, 120°C and 160°C). Details of the post-curing process are displayed in Tab. 3.

Sl. No	Specimen Reference	Epoxy (wt. %)	GNPs (wt. %)	h-BNs (wt. %)
1	PE	100	-	-
2	GNP1	99.9	0.1	-
3	GNP2	99.8	0.2	-
4	GNP3	99.7	0.3	-
5	HBN1	99.7	-	0.3
6	HBN2	99.6	-	0.4
7	HBN3	99.5	-	0.5
8	GH1	99.6	0.2	0.2
9	GH2	99.5	0.25	0.25
10	GH3	99.4	0.3	0.3

Table 2: Test specimen details.

Sl. No	Post Curing Temperature	Specimens
1	80°C	PE + Specimens 2 to 10
2	120°C	PE + Specimens 2 to 10
3	160°C	PE + Specimens 2 to 10

Table 3: Post-curing details.

EXPERIMENTAL DETAILS

The synthesized nanocomposites were evaluated using a range of characterization techniques. The experimental details are as follows.

Material Characterization

- The optical spectroscopic analysis was performed using Raman spectroscopy (LabRAM HR) system. A visible laser wavelength of 514 nm was employed to excite the sample, and a charge-coupled detector (CCD) was used to collect the scattered light. The measurements were conducted at room temperature to ensure stable conditions.
- The chemical composition of the nanocomposites was examined using FTIR spectroscopy (Perkin Elmer System 2000 spectrophotometer). Tests were conducted between 4000 and 500 cm^{-1} to identify functional categories and organic/inorganic components in the sample.
- SEM images of the specimens were captured after coating them with a thin gold film of 10-20 nm thickness to enhance conductivity. The specimens were then examined using a field emission electron microscope (JEOL JSM-63OLA) operating at an accelerating voltage of 5 kV. The sputtering process ensures clear imaging by reducing charging effects during electron beam exposure.

Thermal Tests

- DSC (TA Instruments Q-20) tests were performed by exposing the prepared nanocomposites (Approximately 3-4 mg of the sample was weighed using an electronic scale and was transferred to a testing apparatus) from room temperature gradually at the rate of 10°C/min to 400°C in a pure nitrogen environment. Thermograms obtained from the tests were analyzed with proprietary software.

Mechanical Tests

- Tensile tests were conducted according to ASTM D3039 [16] on rectangular specimens measuring 165 mm × 25 mm × 3 mm. The tests were carried out using a micro UTM (Tinius Olsen) with a 10 kN capacity, maintaining a constant displacement rate of 3 mm/min for all tests.
- Flexural tests were performed on rectangular specimens measuring 120 mm × 13 mm × 3 mm according to ASTM D7264 [17]. The tests were carried out using a micro UTM (Tinius Olsen), with a displacement rate of 3 mm/min using a span length of 50 mm for all trails.
- Impact tests were conducted on unnotched rectangular specimens measuring 70 mm × 13 mm × 3 mm according to ASTM D4812 [18]. The tests were performed using a ZWICK ROELL HIT 50P machine with a nominal work capacity of 5.5 J and a theoretical impact velocity of 3.458 m/s.

Fracture Test

- Fracture tests were conducted according to ASTM D5045 [19] on rectangular specimens measuring 165 mm × 25 mm × 3 mm. The tests were carried out using a micro UTM (Tinius Olsen) with a 10 kN capacity, maintaining a constant displacement rate of 0.5 mm/min for all tests. A saw slit of 0.2 mm thickness was used to machine a crack in the specimens.

The specifications of the test specimens for tensile, flexure impact and fracture tests are depicted in Fig. 1. For all mechanical and fracture tests, 3 samples were tested and an average with standard error was used in plotting the relevant graphs.

Simulation Studies

Finite Element (FE) analysis was used to estimate mechanical properties, which were then validated using experimental test data. The simulation studies were carried out utilizing the ANSYS 2021 R2 software. Nanocomposites were designed using ANSYS Workbench's material designer module by specifying essential parameters such as Young's modulus, Poisson's ratio, and ultimate strength. Tensile and flexural models were meshed using solid 186 elements, which were simulated followed by the application of boundary conditions (BC) [23,24].

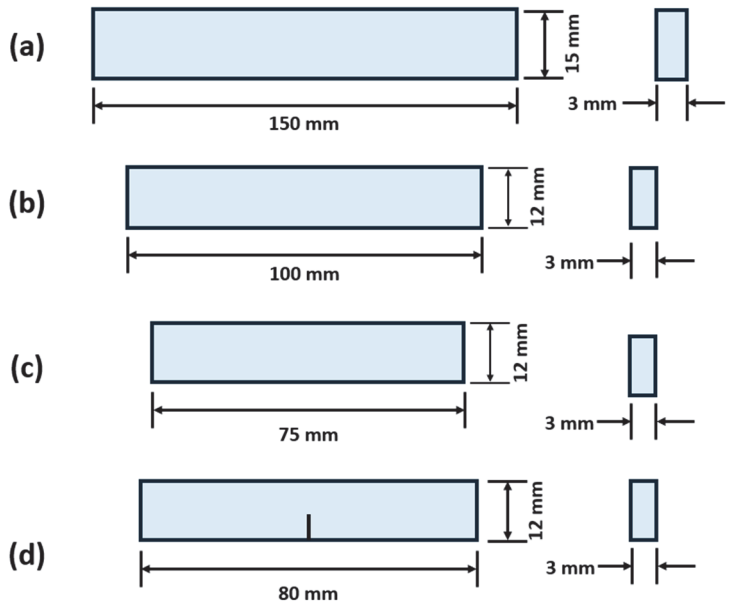

Figure 1: Dimensions of a) Tensile test specimen b) Flexure test specimen and c) Impact test specimen d) Fracture test specimen.

RESULTS AND DISCUSSION

Raman Spectroscopy

The Raman spectroscopy results indicate the presence of epoxide functional groups in the epoxy material under investigation. The characteristic Raman peaks observed at specific wavenumbers, consistent with vibrational modes associated with epoxide moieties, serve as a distinctive signature. These findings provide crucial insights into the molecular composition of the epoxy, confirming the presence of epoxide groups and nanoparticles (GNPs and h-BNs) in the prepared nanocomposites. Fig. 2 shows the Raman spectra of PE, GNP, h-BN and GH-based nanocomposites.

In Raman spectroscopy, the presence of epoxide (or epoxy) functional groups in a material is often characterized by specific vibrational modes associated with the C-O-C bonds in the epoxy ring. C-O-C stretching was observed at 1280-1230 cm^{-1} while C-O-C bending was observed at 800-900 cm^{-1} thus confirming the epoxide presence in the base material [20]. The presence of GNP is witnessed near 1580 cm^{-1} representing the graphitic sp2 carbon-carbon stretching in the G Band followed by the presence of the D band at 1350 cm^{-1} and 2D band at 2700 cm^{-1} [21]. Further, the presence of h-BNs in the prepared composites was witnessed at 1365 cm^{-1} of E2g In-Plane Mode vibration and 800 cm^{-1} wavenumbers of A1g Out-of-Plane Mode, which corresponds to the vibration of boron and nitrogen in a hexagonal lattice [22].

FT-IR

FTIR spectroscopy was also used to evaluate the functional groups of epoxy and nanofillers used in the studies. Fig. 3 shows the FT-IR spectra of PE, GNP, h-BN and GH-based nanocomposites. A characteristic peak for the C-O-C ring stretching vibration in the epoxy group was observed in the range of 850-1000 cm^{-1} and C-O-C Ring Bending was observed around 430-500 cm^{-1} confirming the presence of the epoxy functional group. The presence of GNP in the composite is witnessed

by the presence of G band at 1580 cm^{-1} which corresponds to C-C stretching in graphene. The peaks of (A1g Out-of-Plane Mode) at 800 cm^{-1} correspond to the presence of h-BN in the composite material [22].

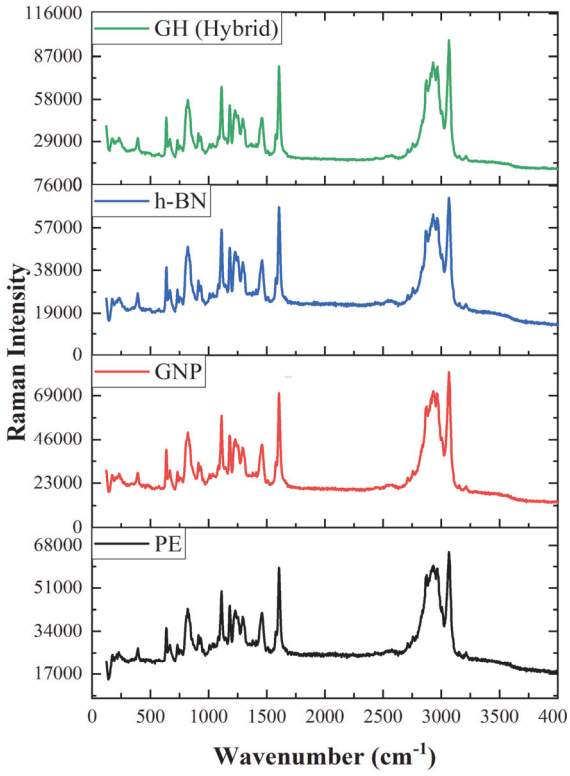

Figure 2: Raman spectra of PE, GNP, h-BN and GH-based nanocomposites.

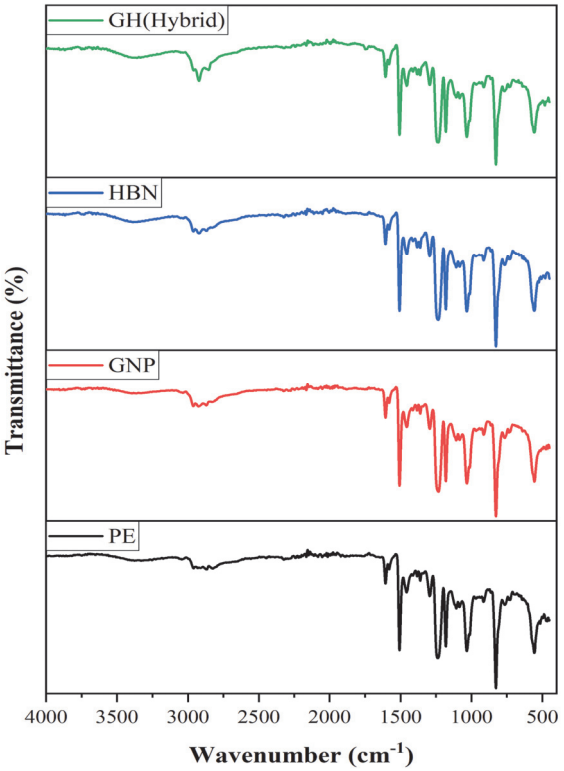

Figure 3: FT-IR spectra of PE, GNP, h-BN and GH-based nanocomposites.

DSC

DSC analysis was performed on select cured and post-cured specimens. The selection of samples for DSC analysis was based on the results from tensile tests, where samples (HBN3, GNP2 and GH3) post cured at 120°C exhibited highest tensile strength in their corresponding configurations. All specimens that were subjected to analysis underwent thermal exposure ranging from ambient to 400°C in a nitrogen environment. Fig. 4 (a) shows the DSC thermographs of cured composites and Fig. 4 (b) shows the DSC thermographs subjected to post-curing (120°C).

The DSC curves show no substantial shift in Tg for room-temperature cured composites (Fig. 4 (a)), as evident from the thermograph the Tg valves of cured composites lay in the range of 63°C to 66°C. The prominent exothermic peaks in the cured specimens have diminished in the post-cured specimens, indicating that post-curing may have completed the reaction or altered the thermal properties. From Fig. 4 (b), the Tg of HBN3, GNP2 and GH3 at 112.85°C, 115.45°C and 110.2°C suggest specific transitions or reactions characteristic of these formulations. The curve shapes indicate that post-curing may have enhanced the thermal stability of the materials since there are fewer variations in heat flow compared to the cured specimens. The average Tg value of the post-cured specimens increases by 174% compared to cured composites. This shift in the DSC curves after post-curing could be due to an increase in the cross-link density or a change in the chemical structure of the composites, leading to different thermal properties. The difference in the DSC curves before and after post-curing can also provide insights into the curing process's kinetics and the post-curing treatment's efficiency [5, 6]. The PE of post-cured specimen shows no significant improvement in the Tg value compared to PE of the cured composite. The thermographs suggest that the addition of GNP and h-BN has a synergistic effect on the thermal behavior of the epoxy composites [26].

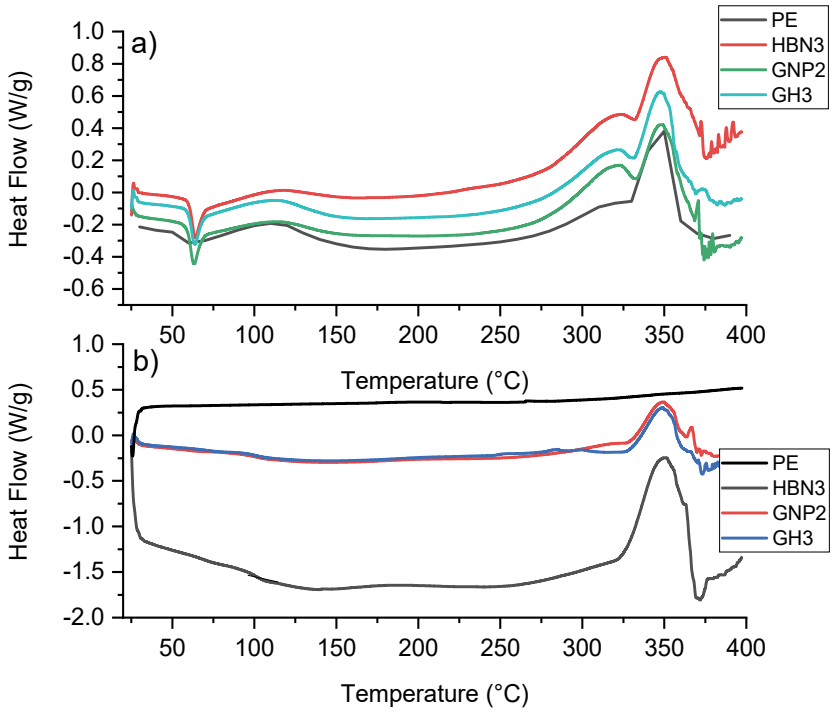

Figure 4: (a) Thermographs of cured composites (b) Thermographs of post-cured composites (120°C).

Tensile Test

This study examines the relationship between reinforcements and the matrix material ultimate stress of PE and various reinforced epoxy specimens subjected to tensile tests after post-curing at three different temperatures: 80°C, 120°C, and 160°C. Fig. 5 shows the variation of ultimate stress in all specimens.

At 80°C post curing PE exhibits tensile stress of 30.7 MPa, GNP1, HBN3 and GH3 showed an increase in stress-bearing capacity by 174% (53.6 MPa), 135% (41.5 MPa) and 157% (48.4 MPa) respectively as compared to PE. This improvement is due to the effective load transmission and strengthening provided by GNPs, HBNs and GH (GNPs + h-BNs) nanofillers within the epoxy matrix respectively. Specimens post-cured at 120°C have fared better tensile load-bearing capacity when compared to PE (40 MPa). This could be due to the increase in Tg of the specimens. Higher Tg increases crosslinking, chain

stiffness, and strong intermolecular interactions resulting in better stress-bearing capacity before failure [15]. GNP1 and HBN3 showed an increase in stress-bearing capacity by 181.5% (72.6 MPa) and 141.0 % (56.4 MPa) respectively compared to PE. At 160°C post curing, a considerable reduction in ultimate stress is observed; this significant drop is due to the thermal instability of the material when exposed to higher post-curing temperature than the Tg limit of the base material (epoxy). However, GNP1 and HBN3 showed an increase in stress-bearing capacity by 202.4% (50.2 MPa) and 210.0 % (52.1 MPa) respectively compared to PE (24.8 MPa). However, GH1 showed a decrease in stress-bearing capacity by 22.8% (when compared to PE at 80°C) due to thermal softening at higher post-curing temperatures [5].

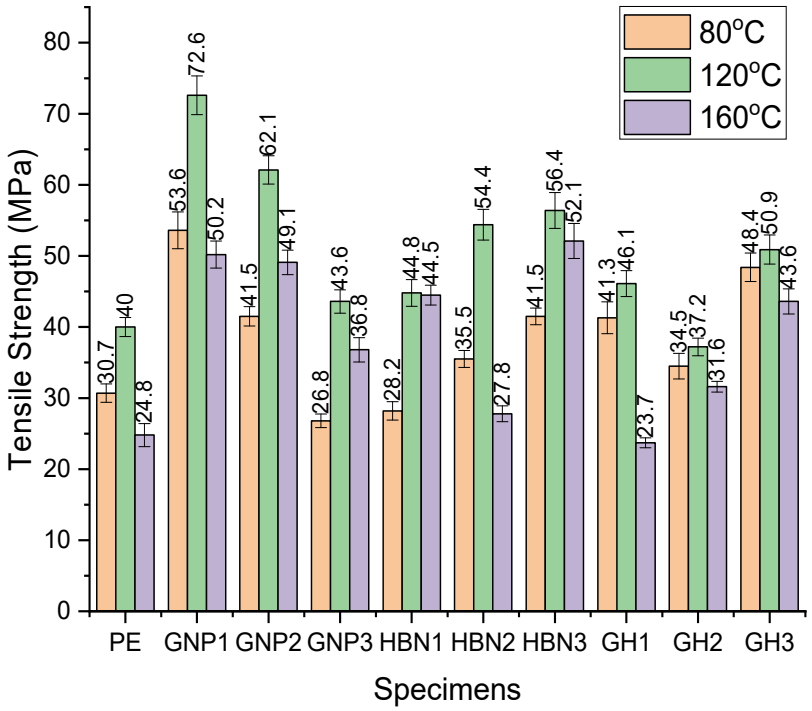

Figure 5: Ultimate Stress v/s Specimens subjected to post-curing temperatures.

SEM analysis

To analyze the surface morphology, dispersion of filler, and their interaction with the matrix, the fractured tensile specimens were examined using SEM. The micrographs of the pure epoxy and one specimen from each nanocomposite configuration were studied and shown in Fig. 6. The specimens exhibiting higher tensile strength among their corresponding filler configuration were selected. From Fig. 6 (a), the pure epoxy surface showed a smooth surface that implies a typical brittle failure. The samples loaded with filers (Fig. 6 (b) – Fig. 6 (c)) exhibited rough surfaces and the cleavage planes were observed. The morphology of GNP nanocomposite (Fig. 6 (b)) exhibits a very rough surface with several cleavage planes, representing regions capable of absorbing fracture energy that results in a higher resistance for crack propagation. The surface of h-BN nanocomposites (Fig. 6 (c)) is relatively smooth and exhibits cleavage planes. The hybrid nanocomposite (Fig. 6 (d)) surface exhibits rough surfaces in some regions and relatively smooth surfaces with cleavage planes in both regions. The higher strength of GNP nanocomposites compared to h-BN and hybrid nanocomposites can be attributed to the higher strength and modulus of GNPs in comparison with h-BN particles [25, 26].

Flexural Test

This study examines the relationship between reinforcements and the matrix material flexural stress of PE and various reinforced epoxy specimens subjected to flexure tests after post-curing at three different temperatures: 80°C, 120°C, and 160°C. Fig. 7 shows the variation of flexural stress in all specimens.

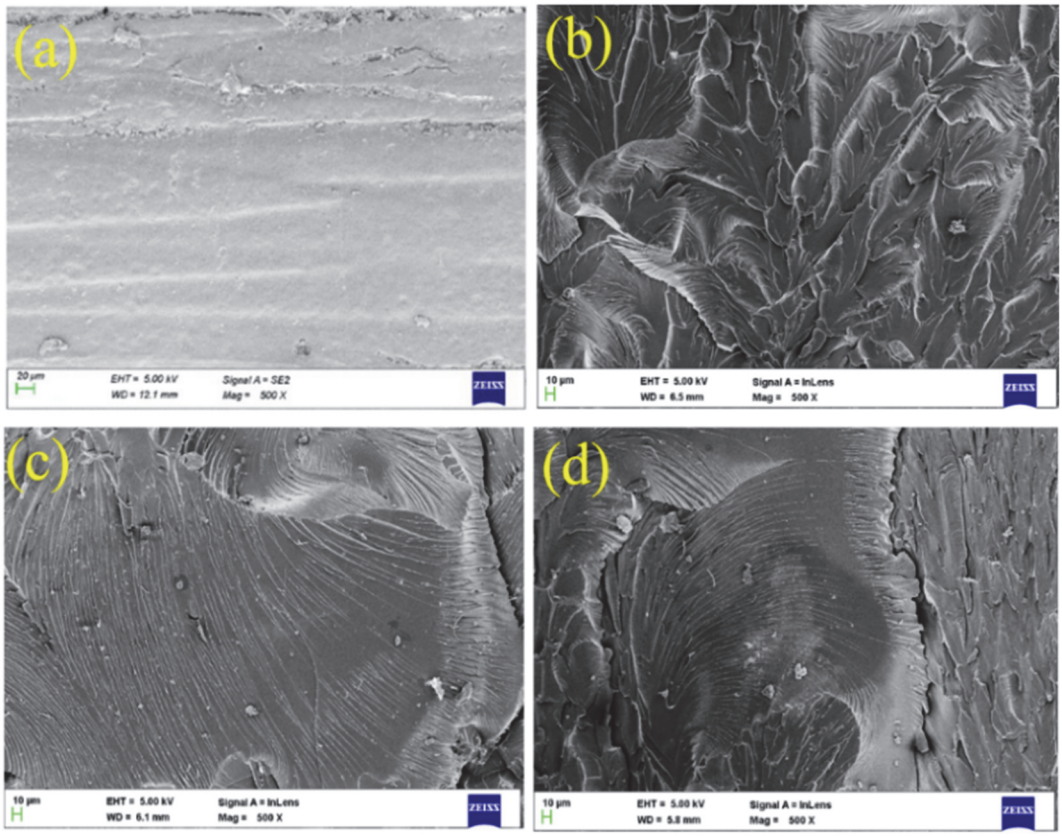

Figure 6: SEM micrographs of (a) Pure epoxy (b) GNP nanocomposite (c) h-BN nanocomposite and (d) Hybrid nanocomposite.

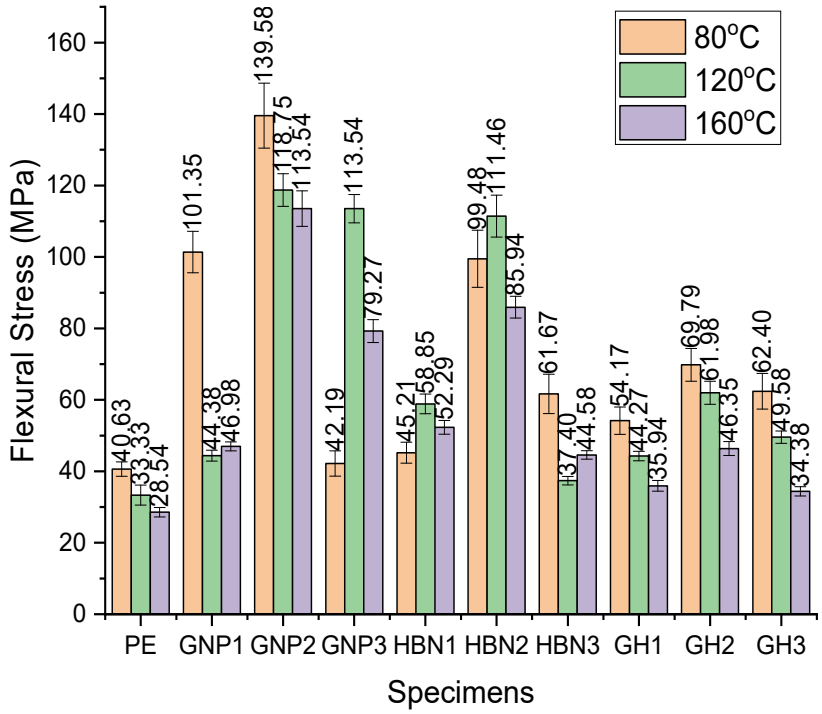

Figure 7: Flexural Stress v/s Specimens subjected to post-curing temperatures.

At 80°C post-curing PE exhibits a flexural stress of 40.63 MPa, GNP2 shows a substantial increase in flexural stress of 139.58 MPa, an increase of 243% compared to PE. This improvement is due to the effective load transmission and strengthening of GNP nanofillers within the epoxy matrix. Specimens post-cured @ 120°C have fared better tensile load-bearing capacity when compared with 80°C (barring GNP2) post-cured specimens and PE, this could be due to the increase in Tg of the specimens. Higher Tg increases crosslinking, chain stiffness, and strong intermolecular interactions resulting in better stress-bearing capacity before failure [15]. GNP2, GNP3 and HBN2 showed an increase in stress-bearing capacity by 256%, 240% and 234 % respectively when compared to PE (33.33 MPa). Specimens post-cured at 160°C, drop in stress-bearing capacity was observed. This is due to the thermal instability of the material when exposed to higher post-curing temperatures than the Tg limit of the base material (epoxy). However, GNP2 and HBN2 showed an increase in stress-bearing capacity by 298% and 201% respectively compared to PE (28.54 MPa) but showed a reduction in bearing strength by 18.6% and 38.4% when compared with GNP2 (of 80°C). GH1 and GH3 showed a decrease in stress-bearing capacity by 11.5% and 15.4% respectively when compared to PE (of 80°C). This decrease is attributed to thermal degradation resulting in a drop in flexural performance [5,6].

Impact Test

This study examines the relationship between reinforcements and the matrix material impact strength of PE and various reinforced epoxy specimens subjected to impact tests after post-curing at three different temperatures: 80°C, 120°C, and 160°C. GNP and h-BN based composites outperformed in absorbing the impact before the break point compared to the PE. This is mainly due to the proper dispersion of NPs in the holding matrix (epoxy) ensuring a stronger interface between them [26]. Fig. 8 shows the impact resistance in terms of impact strength against all specimens subjected to post-curing temperatures.

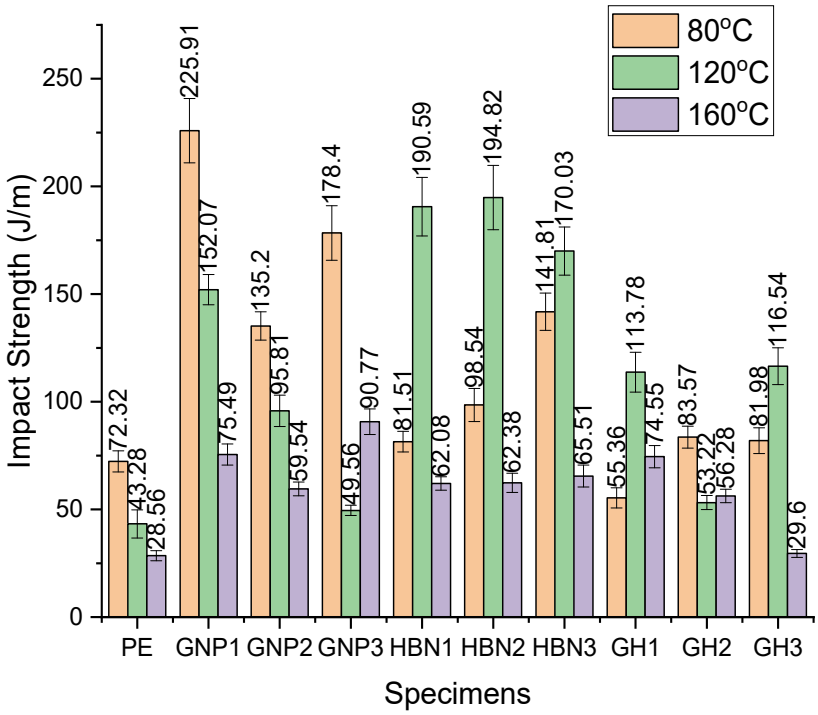

Figure 8: Impact strength v/s Specimens subjected to post-curing temperatures.

At 80°C post curing all specimens (except GH1) exhibited better resistance to impact loading compared to PE (72.32 J/m). This could be related to the material's thermal deterioration limitations, which affect its structural integrity. GNP1 showed an increase in 312% impact resistance when compared with PE. This behavior could be due to efficient interfacial behavior between the GNP and the matrix material. All specimens post-cured at 120°C have exhibited good resistance before failure. HBN1, HBN2 and HBN3 outperformed the impact resistance when compared with GNP reinforced composites, this might be due to the uniform distribution of h-BNs in the matrix material as well as higher glass transition temperature or a composition that resists thermal softening better. Specimens post-cured at 160°C, showed a significant decrease in impact

strength, with only a few specimens maintaining values slightly above that of PE post-cured at 80°C (72.32 J/m). This drop in impact resistance suggests that most test specimens have had higher crosslinking reactions leading to brittle nature [26].

Fracture Test

The fracture test investigates the relationship between reinforcements and the matrix material fracture strength of PE and various reinforced epoxy specimens subjected to post-curing at three different temperatures: 80°C, 120°C, and 160°C. Fig. 9 shows the fracture toughness against all specimens subjected to post-curing temperatures.

The fracture toughness of PE specimen post-cured at 80°C is 2.86 MPa.m$^{1/2}$ and is used as a reference for comparison. GNP reinforced composites perform well due to strong bonding with epoxy matrix. GNP2 showed an increase in fracture toughness by 60% when compared with PE. Specimens post-cured at 120°C, showed further improvement in fracture strength, particularly in h-BN reinforced samples. This improvement is because of the uniform dispersion of h-BN and its higher glass transition temperature, enhancing fracture resistance. However, specimens post-cured at 160°C, exhibited a significant reduction in fracture strength, indicating thermal degradation. All nanocomposites (Except GH3) post-cured at 160 C exhibited an increase in fracture toughness compared to PE [13, 24].

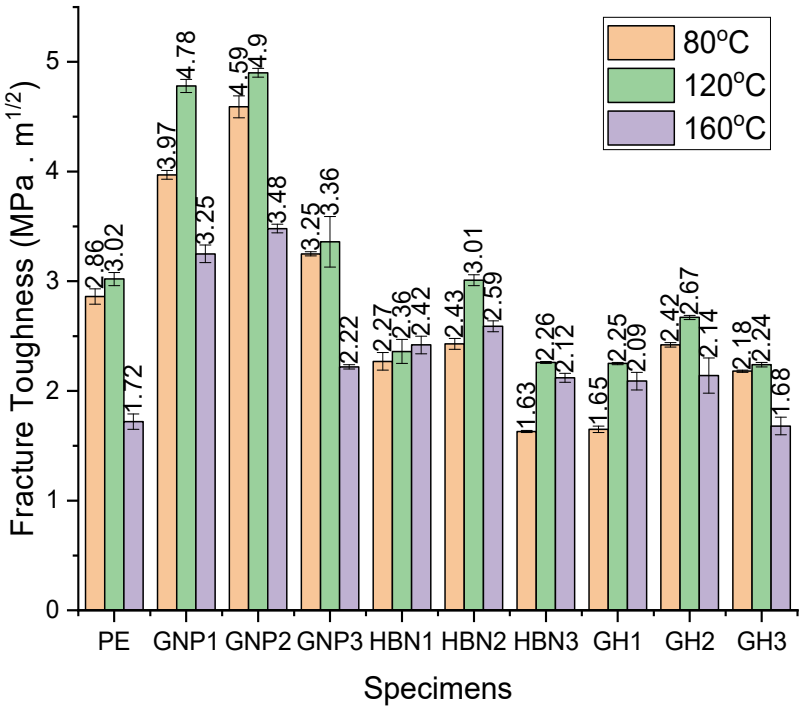

Figure 9: Fracture toughness v/s Specimens subjected to post-curing temperatures.

Simulation Studies – Creation of material and model

In the material designer module of Ansys Workbench, a new material was developed in the engineering data section, as illustrated in Fig. 10 (a). Basic properties, such as Young's modulus, Poisson's ratio, and ultimate strength, derived from tensile tests and flexural tests were employed to create the matrix material [23]. Additional elasticity properties, including bulk modulus and shear modulus, were determined using the built-in methods provided by the material designer. Representative volume elements (RVEs) were generated for each GNP1, HBN3, and GH3 of tensile models and GNP2, HBN2, and GH2 of flexural models. The mechanical properties of epoxy, GNP, and h-BN, detailed in Tab. 1, were utilized to construct the RVEs, the meshing of RVEs is depicted in Fig. 10 (b). This material was used as input for structural analysis in ANSYS Workbench. 3D models for tensile and flexural test analysis were created in SolidWorks using the specifications provided in Fig. 1 [24].

Mesh generation and boundary conditions

The tensile and flexural models were meshed with Solid 186 element as shown in Figs. 11 (a) & 11 (b) respectively. The BC of tensile tests was done with one end clamped, and axial force was applied on the other end, as shown in Fig. 12 (a). The

BC of flexural tests was done with two ends clamped and an axial force was applied in the mid-span of the test specimen as shown in Fig. 12 (b) [23, 24].

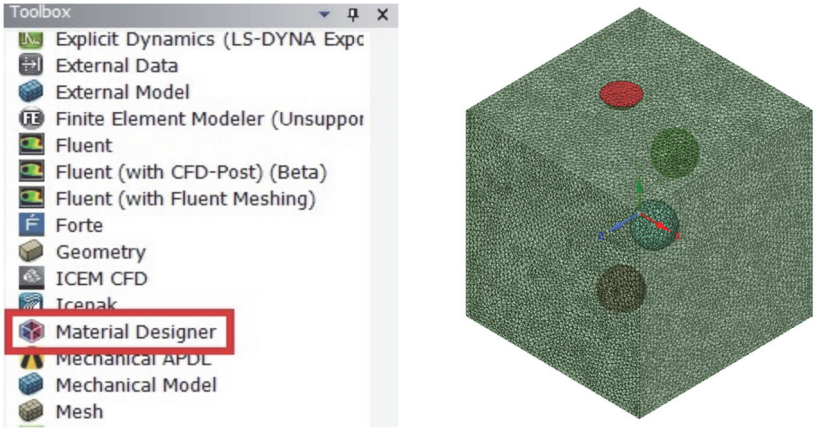

Figure 10: (a) Material Designer module (b) RVE created in Material Designer.

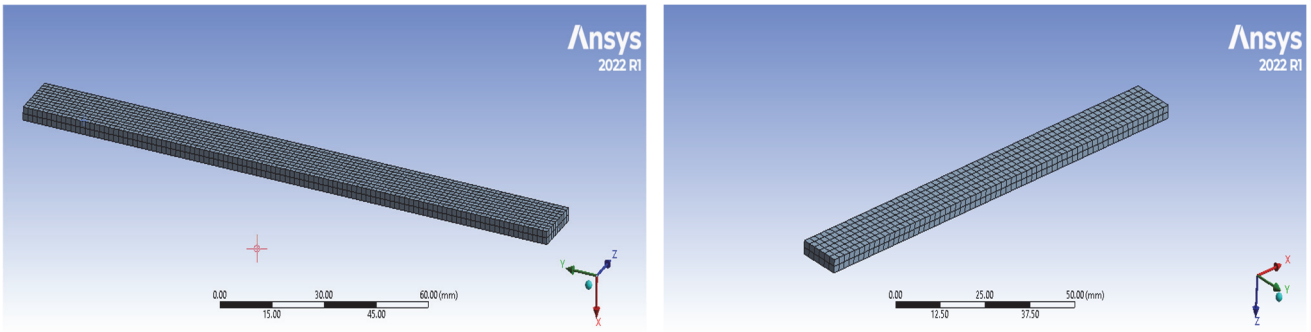

Figure 11: (a) Tensile model mesh (b) Flexural model

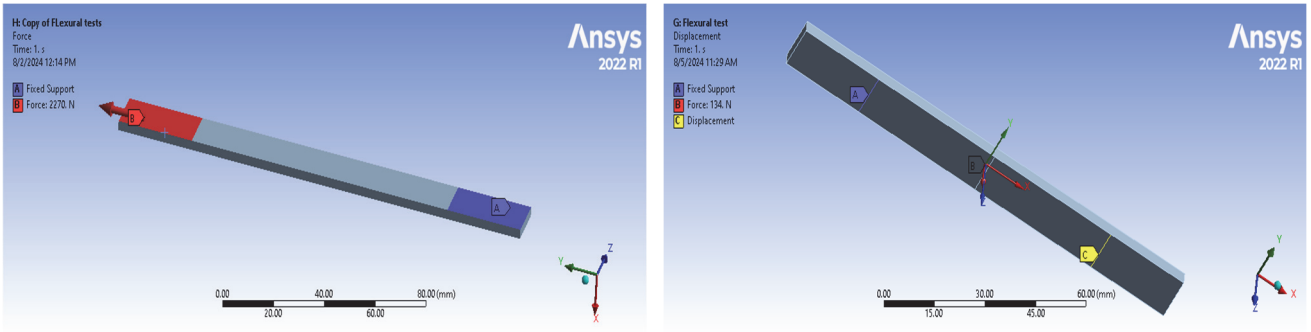

Figure 12: (a) Tensile model BC (b) Flexural model BC

Simulation Results

Figs. 13 (a), 14 (a), and 15 (a) represent the simulated tensile test results of GNP1, HBN3 and GH3 specimens respectively. Figs. 13 (b), 14 (b) and 15 (b) represent the simulated flexural results of GNP2, HBN2 and GH2 specimens respectively. Tab. 4 illustrates the simulated v/s experimental results of the tensile and flexural models. Overall, the variations in both tensile and flexural tests between experimental and simulated results for all nanocomposites remained within the acceptable range of 20% [15].

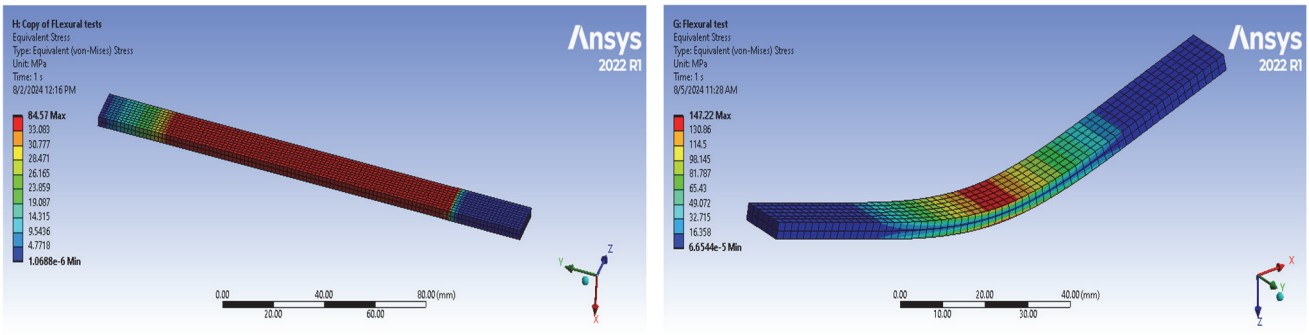

Figure 13: (a) GNP1 tensile model (b) GNP2 flexural model

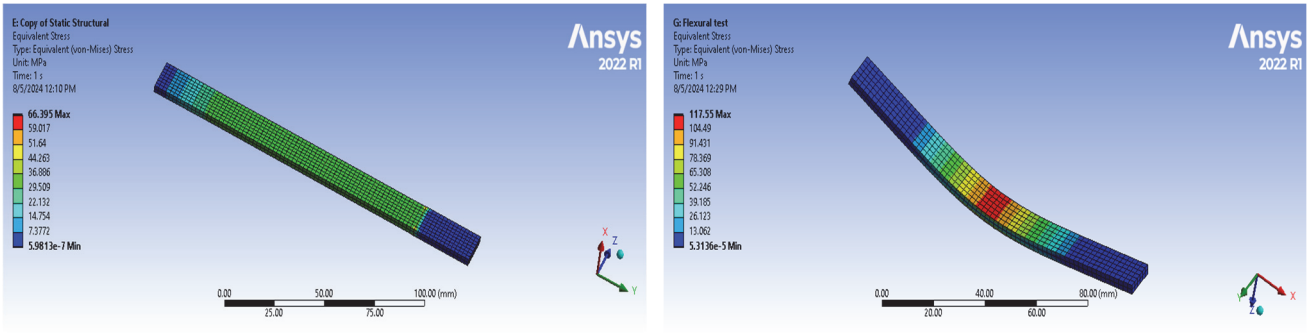

Figure 14: (a) HBN3 tensile model (b) HBN2 flexural model

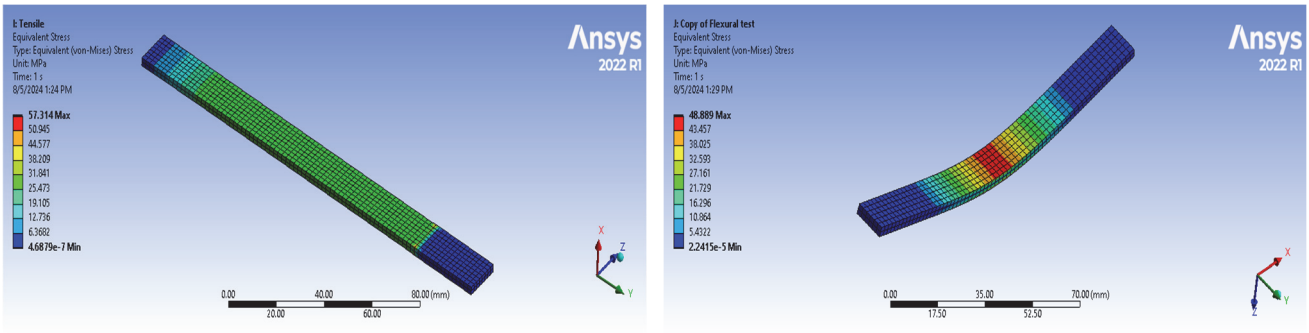

Figure 15: (a) GH3 tensile model (b) GH2 flexural model

Specimen	Simulated tensile strength (MPa)	Experimental tensile strength (MPa)	Variation in results (%)	Specimen	Simulated flexural strength (MPa)	Experimental flexural strength (MPa)	Variation in results (%)
GNP1	84.57	72.6	16.48	GNP2	147.22	139.58	5.47
HBN3	66.39	56.4	17.71	HBN2	117.55	111.46	5.46
GH3	57.31	50.9	12.6	GH2	48.88	46.35	5.45

Table 4: Simulated v/s Experimental results of tensile and flexure tests.

Conclusions

The study confirms the incorporation of GNP and h-BN nanofillers in an epoxy matrix improves their mechanical properties, such as tensile, flexural, and impact strength. This enhancement is due to increased interfacial adhesion between the nanofillers and the epoxy matrix. The epoxy composites infused with varied concentrations of GNPs

and h-BN were evaluated, demonstrating that changing the nanofiller content can successfully customize the composite's mechanical, fracture, and thermal properties to match specific application requirements.

The multi-filler system, which included GNP and h-BN, outperformed PE in terms of mechanical, fracture, and thermal properties. During tensile loading, GNP1 at 120°C absorbed 136% more stress before failing, and GNP2 at 80°C absorbed 243% more flexural loading. Similarly, GNP1 at 80°C required 212% greater impact stress before failing, whereas GNP2 at 120°C showed a 71% increase in resistance to failure. FTIR, SEM and Raman spectroscopy were used to confirm the presence and dispersion of nanofillers in the epoxy matrix, providing more information about the composite structure and filler-matrix interactions.

It has also been found that post-curing temperatures substantially impact the composite's mechanical and thermal properties. Specimens post-cured at 120°C showed improved mechanical and thermal performance, particularly in Tg and tensile strength. These improved nanocomposite materials indicate a considerable promise for high-performance applications in aerospace and automotive space where durability and thermal resistance are crucial. Furthermore, simulation analysis using ANSYS software showed a high match with experimental results, with variances falling within a 20% range.

ACKNOWLEDGMENT

The authors gratefully acknowledge the organization for providing the essential facilities at the Center for Materials Science and the School of Mechanical Engineering, KLE Technological University, Hubballi, Karnataka, India.

REFERENCES

[1] Shundo, A., Yamamoto, S. and Tanaka, K. (2022). Network formation and physical properties of epoxy resins for future practical applications. Jacs Au, 2(7), pp.1522-1542, DOI: 10.1021/jacsau.2c00120.

[2] Dallaev, R., Pisarenko, T., Papež, N., Sadovský, P. and Holcman, V. (2023). A brief overview on epoxies in electronics: properties, applications, and modifications. Polymers, 15(19), p.3964, DOI: 10.3390/polym15193964.

[3] Karak, N. (2021). Overview of epoxies and their thermosets. In Sustainable epoxy thermosets and nanocomposites (pp. 1-36). American Chemical Society, DOI: 10.1021/bk-2021-1385.ch001.

[4] Seidlová, M., Hodul, J., Žižková, N. and Borg, R.P. (2023). Possibilities of influencing the crystallization process of bisphenol a-and bisphenol f-based epoxy resins used for hydrophobic coatings on concrete. Polymers, 15(19), p.3871, DOI: 10.3390/polym15193871.

[5] Sambayi, P.M.K. and Heyns, P.S. (2023). Effects of multiple post cure cycles on properties of composite carbon fibre and epoxy materials. Journal of Composite Materials, 57(15), pp.2467-2481, DOI: 10.1177/00219983231169333.

[6] Capricho, J.C., Fox, B. and Hameed, N. (2020). Multifunctionality in epoxy resins. Polymer Reviews, 60(1), pp.1-41, DOI: 10.1080/15583724.2019.1650063.

[7] Moller, J.C., Berry, R.J. and Foster, H.A. (2020). On the nature of epoxy resin post-curing. Polymers, 12(2), p.466. DOI: 10.3390/polym12020466.

[8] Lascano, D., Quiles-Carrillo, L., Torres-Giner, S., Boronat, T. and Montanes, N. (2019). Optimization of the curing and post-curing conditions for the manufacturing of partially bio-based epoxy resins with improved toughness. Polymers, 11(8), p.1354, DOI: 10.3390/polym11081354.

[9] Olszowska, K., Godzierz, M., Pusz, S., Myalski, J., Kobyliukh, A., Georgiev, G., Posmyk, A., Tsyntsarski, B. and Szeluga, U. (2023). Development of epoxy composites with graphene nanoplatelets and micro-sized carbon foam: Morphology and thermal, mechanical and tribological properties. Tribology International, 185, p.108556, DOI: 10.1016/j.triboint.2023.108556.

[10] Wong, T.L., Vallés, C., Nasser, A. and Abeykoon, C. (2023). Effects of boron-nitride-based nanomaterials on the thermal properties of composite organic phase change materials: A state-of-the-art review. Renewable and Sustainable Energy Reviews, 187, p.113730, DOI: 10.1016/j.rser.2023.113730.

[11] Lawal, S.A., Medupin, R.O., Yoro, K.O., Okoro, U.G., Adedipe, O., Abutu, J., Tijani, J.O., Abdulkareem, A.S., Ukoba, K., Ndaliman, M.B. and Sekoai, P.T. (2023). Nanofluids and their application in carbon fibre reinforced plastics: A review of properties, preparation, and usage. Arabian Journal of Chemistry, 16(8), p.104908, DOI: 10.1016/j.arabjc.2023.104908.

[12] Choukimath, M.C., Banapurmath, N.R., Patil, A.Y., Hemadri, S. and Jalawadi, A.R. (2020). Light weight polymer Nano composites reinforced with h-BN for high temperature applications. In IOP Conference Series: Materials Science and Engineering (Vol. 872, No. 1, p. 012112). IOP Publishing, DOI: 10.1088/1757-899X/872/1/012112.
[13] Jahani, Y., Baena, M., Barris, C., Perera, R. and Torres, L., 2022. Influence of curing, post-curing and testing temperatures on mechanical properties of a structural adhesive. Construction and Building Materials, 324, p.126698, DOI: 10.1016/j.conbuildmat.2022.126698.
[14] Min, C., Sun, Z., Li, Q., Yu, H., Xu, Z. and Liang, H. (2023). Three-dimensional interconnected graphene architecture reinforced epoxy composite with superior mechanical and tribological properties. Journal of Materials Research and Technology, 27, pp.2563-2576, DOI: 10.1016/j.jmrt.2023.10.099.
[15] Choukimath, M.C., Banapurmath, N.R., Riaz, F., Patil, A.Y., Jalawadi, A.R., Mujtaba, M.A., Shahapurkar, K., Khan, T.Y., Alsehli, M., Soudagar, M.E.M. and Fattah, I.M.R. (2022). Experimental and computational study of mechanical and thermal characteristics of h-BN and GNP infused polymer composites for elevated temperature applications. Materials, 15(15), p.5397, DOI: 10.3390/ma15155397.
[16] ASTM D3039/D3039M-17, Standard Test Method for Tensile Properties of Polymer Matrix Composite Materials. ASTM International: West Conshohocken, PA, USA, 2014. DOI: 0.1520/D3039_D3039M-08.
[17] ASTM D7264/D7264M-21, Standard Test Method for Flexural Properties of Polymer Matrix Composite Materials ASTM International: West Conshohocken, PA, USA, 2021. DOI: 10.1520/D7264_D7264M-21.
[18] ASTM D4812-19e1, Standard Test Method for Unnotched Cantilever Beam Impact Resistance of Plastics. ASTM International: West Conshohocken, PA, USA, 2022. DOI: 10.1520/D4812-19E01.
[19] ASTM D5045-14R22, Standard Test Methods for Plane-Strain Fracture Toughness and Strain Energy Release Rate of Plastic Materials. ASTM International: West Conshohocken, PA, USA, 2022. DOI: 10.1520/D5045-14R22.
[20] Smith, B. (2022). The Infrared Spectra of Polymers V: Epoxies. Spectroscopy, 37(3), pp.17-19, DOI: 10.56530/spectroscopy.mg2473z4.
[21] Dovbeshko, G., Cherepanov, V., Boiko, V., Perederiy, A., Olenchuk, M., Negriyko, A., Posudievsky, O., Moiseyenko, V. and Romanyuk, V. (2022). Raman modes and mapping of graphene nanoparticles on Si and photonic crystal substrates. Optical Materials: X, 15, p.100163, DOI: 10.1016/j.omx.2022.100163.
[22] Cui, M., Ren, S., Qin, S., Xue, Q., Zhao, H. and Wang, L. (2017). Non-covalent functionalized hexagonal boron nitride nanoplatelets to improve corrosion and wear resistance of epoxy coatings. RSC advances, 7(70), pp.44043-44053, DOI: 10.1039/c7ra06835b.
[23] Nimbagal, V., Banapurmath, N.R., Umarfarooq, M.A., Revankar, S., Sajjan, A.M., Soudagar, M.E.M., Shahapurkar, K., Alamir, M.A., Alarifi, I.M. and Elfasakhany, A. (2023). Mechanical and fracture properties of carbon nano fibers/short carbon fiber epoxy composites. Polymer Composites, 44(7), pp.3977-3989, DOI: 10.1002/pc.27371.
[24] Dileep, K., Srinath, A., Banapurmath, N.R., Umarfarooq, M.A. and Sajjan, A.M. (2023). Mechanical and fracture characterization of epoxy/PLA/graphene/SiO2 composites. Frattura ed Integrità Strutturale, 17(64), pp.229-239. DOI: 10.3221/IGF-ESIS.64.15.
[25] Hardis, R., Jessop, J.L., Peters, F.E. and Kessler, M.R. (2013). Cure kinetics characterization and monitoring of an epoxy resin using DSC, Raman spectroscopy, and DEA. Composites Part A: Applied Science and Manufacturing, 49, pp.100-108, DOI: 10.1016/j.compositesa.2013.01.021.
[26] Zafeiropoulou, K., Kostagiannakopoulou, C., Geitona, A., Tsilimigkra, X., Sotiriadis, G. and Kostopoulos, V. (2021). On the Multi-Functional Behavior of Graphene-Based Nano-Reinforced Polymers. Materials, 14(19), p.5828, DOI: 10.3390/ma14195828.